Conf-940553--84 SAND94-0323C

To be published in the Proceedings of the 1994 International Conference on High Level Radioactive Waste Management, Las Vegas, NV, May 22-26, 1994.

DETAILED CHARACTERIZATION AND PRELIMINARY ADSORPTION MODEL FOR MATERIALS FOR AN INTERMEDIATE-SCALE REACTIVE-TRANSPORT EXPERIMENT

David B. Ward and Charles R. Bryan
Dept. of Earth and Planetary Sciences
University of New Mexico
Albuquerque, NM 87131-1116
(505) 277-4204

Malcolm D. Siegel
Chemical Processes Dept. 6119
Sandia National Laboratories,
Albuquerque, New Mexico 87158-0701
(505) 844-5426

ABSTRACT

An intermediate-scale transport-model experiment, involving the migration of fluid and tracers (Li, Br, Ni) through a 6-m-high × 3-m-diameter caisson filled with Wedron 510 sand, is being carried out for the Yucca Mountain Site Characterization Project. The surface chemistry of the sand has been studied and a preliminary surface-complexation model of Ni adsorption has been formulated for use in transport calculations. XPS and leaching studies suggest that the surface of the quartz sand is partially covered by thin layers of Fe-oxyhydroxide and Ca-Mg carbonate and by flakes of kaolinite. Ni adsorption by the sand is strongly pH-dependent, showing no adsorption at pH 5 and near-total adsorption at pH 7. The location of the adsorption edge is independent of ionic strength and the concentration of dissolved Ni; it is shifted to slightly lower pH with higher P_{CO_2} and to slightly higher pH by competition with Li. Diminished adsorption at alkaline pH with higher P_{CO_2} implies formation of dissolved Ni-carbonato complexes. Ni adsorption edges for goethite and quartz, two components of the sand were also measured. Ni adsorption on pure quartz is only moderately pH-dependent and differs in shape and location from that of the sand, whereas Ni adsorption by goethite is strongly pH-dependent. A triple-layer surface-complexation model developed for goethite provides a good fit to the Ni-adsorption curve of the sand. Based on this model, the apparent surface area of the Fe-oxyhydroxide coating is estimated to be ~560 m^2/g, compatible with its occurrence as amorphous Fe-oxyhydroxide. Potentiometric titrations on the sand also differ from those of pure quartz and suggest that the effective surface area of the sand may be significantly greater than that measured by N_2-BET gas adsorption. Attempts to model the adsorption characteristics of the bulk sand in terms of the properties of pure end member components suggest that much of the sand surface is inert. Although the exact mechanisms of Ni adsorption remain ambiguous, this preliminary adsorption model provides an initial set of parameters that can be used in transport calculations.

I. INTRODUCTION

Integrated flow and transport experiments are being carried out as part of the reactive transport model validation program of the Yucca Mountain Site Characterization Project.[1] Major issues that are being addressed include: (1) What geochemical characteristics of the fractured and porous media will dominate chemical retardation of radionuclides? (2) What are the primary contributors to the uncertainty in the accurate detection of the tracers in field transport experiments? and (3) Which retardation models adequately describe tracer and radionuclide migration?

An intermediate-scale transport-model validation experiment is being carried out at the Experimental Engineered Test Facility at Los Alamos National Laboratory. The experiment involves the detection and prediction of the migration of fluid and tracers (Li, Br, Ni) through a 6-m-high × 3-m-diameter caisson filled with Wedron 510 sand, a commercially available silica sand (Wedron Silica, Wedron, IL 60557). The overall objectives, experiment plan, and materials characterization studies are described in recent publications.[2,3,4] The caisson experiment provides a relatively simple framework for data collection and model development for the validation of reactive transport models. The results of the transport experiments with these tracers and minerals will have applications to other studies in the Yucca Mountain Site Characterization Project (YMP). Nickel is representative of radionuclides released from the structural components of the spent fuel rods in high-level waste and is considered an important waste element due its relatively low

DISCLAIMER

DISCLAIMER

Portions of this document may be illegible in electronic image products. Images are produced from the best available original document.

retardation in Yucca Mountain tuffs. The component minerals of the caisson sand (quartz, calcite and iron oxyhydroxides) are present in fractures in Yucca Mountain tuffs.

According to its bulk chemistry and mineralogy, Wedron 510 sand is nearly pure quartz, but preliminary characterization[2,3] suggested that it contains at least three other chemically reactive components: carbonate, iron oxyhydroxide, and kaolinite. Optical and mechanical analyses indicated that Wedron 510 sand is composed of rounded grains of quartz and rare accessory minerals. A 5-point N_2-BET (Brunauer, Emmet, and Teller[5]) isotherm indicated a surface area of 0.12 m^2/g, but the data were somewhat scattered. Surface mineralogy, inferred from leaching experiments and anomalous titration behavior, included Fe-oxyhydroxide and Ca+Mg carbonate. Kaolinite and quartz were identified by X-ray diffraction in a colloidal fraction that appeared at pH > 8.5. Examination of the sand by scanning electron microscopy (SEM) failed to reveal any grains or particles rich in Fe or Ca+Mg, even in the colloidal fraction, implying that the sources of these elements (Fe-oxyhydroxide and carbonate) occur as thin coatings or as fine particles adhering to the grains of sand. Several questions important to modeling retardation for the caisson experiment are related to the role of the minor phases in the overall adsorption behavior of the sand: (1) Are the minor phases present as surface coatings or discrete particles? (2) What will be the effects of dissolution of the minor minerals on the chemical compositions of the pore water and mineral surfaces and on the behavior of the tracers? (3) Can the adsorptive characteristics of the bulk sand mixture be modeled in terms of the properties of pure end-member components?

The work presented in this paper represents the product of the *detailed characterization* phase of the caisson experiment.[2] During this phase, data describing the interactions between each tracer and the sand, among the tracers, and among the tracers and the other solutes in the pore water of the sand are being collected to allow application of several models of geochemical retardation. These include batch distribution coefficients (K_d 's), adsorption isotherms, and surface-complexation constants. Analysis of the sand surface by X-ray photoelectron spectroscopy (XPS) and potentiometric titrations, and studies of Ni solubility and adsorption by the sand are described in this paper. In the *predictive modeling* and *flow and transport test* phases of the caisson experiment, K_d data will be used to calculate tracer transport with the FEHMN[6] code, and surface-complexation constants will be used in the LEHGC version of the HYDROGEOCHEM[7] code.

II. METHODS

A. Surface Analysis

1. Surface Preparation. Acid washed samples were prepared by boiling raw Wedron 510 sand or Min-U-Sil 5 quartz in 6 N HCl for 4 h to clean surfaces of all carbonate and Fe-oxyhydroxide coatings. After cooling, the supernate was decanted, and the samples were rinsed repeatedly with air-saturated water (conductivity > 10 MΩ before adding air) until the pH of the rinse water reached 5.6. Finely powdered samples were stored as suspensions in deionized water, whereas granular samples were dried.

2. X-ray Photoelectron Spectroscopy. Both untreated and leached grains of Wedron 510 sand were examined by X-ray photoelectron spectroscopy (XPS) using a VG Microtech CLAM2 instrument. Mounts were prepared by densely packing grains on a platform coated with double-sided tape. Under vacuum, the platform was exposed to Al K_α X-rays. Secondary photoelectrons passed through a 4 × 10 mm slit and were decelerated to 50 eV before entering the detector.

3. Potentiometric Titration. Potentiometric surface titrations were carried out using an automated instrument made by George Redden of Stanford University. Computer-controlled 2.5 m*l* micrometer syringes added acid or base to a stirred 250 m*l* polypropylene reactor vessel. The pH was monitored by a combination electrode located in the reactor. When analyzing coarse materials that settled rapidly (i.e., sand), the electrode was shielded from the direct flow to avoid discrepancies induced by the sedimentation potential.[8] The pH was considered to be stable when six pairs of readings differing by < 0.15 mV had been accumulated. The headspaces of the reactor and the basic reagent bottle were continuously purged with de-acidified and humidified Ar; the reactor temperature was the same as the ambient laboratory temperature (23 – 25°C).

After vigorously stirring the suspension for at least 45 min while under Ar purge to remove all dissolved CO_2, acid was added (if necessary) to provide an initial pH near 4. The suspension was then incrementally titrated to an endpoint of pH 9 using 0.05 M NaOH, and the ionic strength at the endpoint was measured by comparing conductivity with NaCl standards. Acid was then added to

return the suspension to its initial pH, solid NaCl was added to raise the ionic strength, the suspension was stirred vigorously for 10 min to flush out any CO_2 that may have entered, and the incremental titration was repeated. Corrections to the experimental data for total electrolyte volume and ionic strength were calculated at each step of a titration.

A system consisting of 150 g acid-washed Wedron 510 sand and 150 m*l* electrolyte was titrated over the pH range 4.5 – 9 at ionic strengths ranging from 0.0003 to 0.096 M. Acid-washed Min-U-Sil 5 α-quartz was also potentiometrically titrated to provide a baseline for validating the experimental procedure and to provide a point of reference for titrations on acid-washed Wedron sand. The titrated system consisted of 4.534 g HCl-washed Min-U-Sil 5 and 150 m*l* NaCl electrolyte. It was continuously titrated over the pH range 4.2 – 9 at ionic strengths ranging from 0.0003 to 0.096 M.

B. Batch Solubility and Adsorption Studies

1. Solubility Studies of Ni Hydroxides. Total dissolved Ni was measured as a function of pH in nominally CO_2-free supersaturated batch systems lacking adsorbent to determine the solubility of $Ni(OH)_2$ in the background electrolyte. Batch systems containing 30 m*l* 0.001 M NaCl electrolyte and 1 – 7600 μg/m*l* ($1.7 \cdot 10^{-5}$ to $1.3 \cdot 10^{-1}$ M) total Ni were equilibrated for 14 days over the pH range 7 – 10 in 50 m*l* polyallomar centrifuge tubes. To obtain reliable and consistent pH values, CO_2-free conditions were maintained as described below for batch-adsorption studies.

Systems were initially supersaturated with respect to amorphous $Ni(OH)_2$ by at least a factor of three, based on the equilibrium constants of Baeyens and McKinley[9]. For systems with a target pH of less than 8, Ni was added as $NiCl_2 \cdot 6H_2O$ to provide initial concentrations in the range 760 – 7600 μg/m*l* (0.013 – 0.13 M). For more alkaline systems (pH > 8), an aliquot of 1000 μg/m*l* Ni standard was added to provide an initial concentration of 1 μg/m*l* ($1.7 \cdot 10^{-5}$ M). Nickel concentrations were determined by GFAA as described below.

Macroscopic quantities of precipitate formed in tubes with the highest Ni concentrations (pH < 8). The precipitate was collected by vacuum filtration on a 0.4 μm polycarbonate membrane filter and washed with a few m*l* of methanol before air-drying. It was analyzed by X-ray diffraction using a powder mount on an oriented quartz crystal scanned over a 2θ range of 5° – 65°. Phase identification was accomplished visually by overlaying the diffractogram with a stick-figure representation of the expected maxima for candidate minerals.

2. Batch Adsorption Studies. Batch adsorption studies were carried out in 0.001 M NaCl electrolyte using substrates of Wedron 510 sand (Wedron Silica, Wedron, IL), synthesized goethite[10,11] or Min-U-Sil 5 α-quartz (U.S. Silica, Pittsburgh, PA). Reaction vessels were 50 m*l* Oak Ridge-style centrifuge tubes made of either polyallomar of polycarbonate with polypropylene screw caps. Batch systems consisted of 20 m*l* electrolyte and 20 g sand, 0.4467 g Min-U-Sil, or 2.353 mg goethite.

Prior to addition of adsorbate, the pH of each suspension was adjusted using dilute HNO_3 and NaOH solutions, and the tubes were equilibrated for 2 – 3 days. The suspensions were then spiked with a pH-neutral Ni solution and re-equilibrated for 2 – 4 days. Total added Ni concentrations were 100 – 200 ng/m*l* ($1.7 - 3.4 \cdot 10^{-6}$ M). In two sets, Li was also added as a pH-neutral LiBr solution; total added Li concentrations were 10 – 17 μg/m*l* ($1.4 - 2.5 \cdot 10^{-3}$ M).

In nominally CO_2-free experiments, the electrolyte was sparged with Ar, the headspace in the centrifuge tubes was filled with Ar, and pH was measured under Ar atmosphere. The tubes were equilibrated on the benchtop surrounded by air, or in a glovebox filled with nitrogen. In other experiments that were partially equilibrated with atmospheric CO_2, initial pH adjustment was carried out in air followed by sparging with air for 10 – 15 min, equilibration for two days, and then sparging again with air before Ni was added. The batch systems were equilibrated in closed tubes in the ambient atmosphere, and final pH measurements were made under a static Ar atmosphere. During equilibration for all experiments, the tubes were agitated gently on hematology mixers.

C. Chemical Analysis

Aliquots for Ni analysis were filtered through 0.2 μm nylon syringe filters and acidified to 2% (0.32 M) HNO_3. Nickel concentrations were determined using graphite-furnace atomic absorption spectroscopy (GFAA) on a Perkin-Elmer 5000 instrument with HGA-500 graphite-furnace controller and AS-1 auto-sampler. The data-reduction scheme fit a quadratic curve to the absorbance data and applied corrections for carryover of Ni in the furnace tube and for evaporation from the auto-sampler vials, achieving better than ± 1.8% (1 s.d.) precision over

a dynamic range of 0 – 200 ng/ml, with a limit of detection of 0.2 ng/ml.

Measurements of pH were made using an Orion ROSS 8102 combination-pH electrode and Orion 940 pH meter. The electrode was allowed to equilibrate with the solution being measured until the electrode drift rate was less than 2 mV/min. Because samples typically contained a partial pressure of CO_2 less than atmospheric, the headspace of each vessel was purged with acid-free humidified Ar before agitation and measurement. Measurements were performed under a static Ar atmosphere.

III. RESULTS

A. X-ray Photoelectron Spectroscopy

X-ray photoelectron spectroscopy (XPS) provides information about elemental composition and chemical speciation for a thin (~5 nm) surface layer.[12] X-ray photoelectron spectra were acquired on both untreated and acid-washed sand. The acid-washed sand had also been used in a titration experiment; a colloidal component (presumably kaolinite) was liberated at high pH and subsequently rinsed away. For the untreated sand, Si was the dominant cation, followed by Al (0.28 abundance relative to Si), and subequal amounts of Ca and Mg (0.02 – 0.03 abundance relative to Si). Reducing the slit width showed that the minor phases must have been uniformly distributed rather than occurring as rare large single grains. The acid-washed sand had 90% less Al and no Ca or Mg. Interfering peaks from the mounting tape obscured the possible presence of Fe and CO_3^{2-} in both samples.

In the untreated sand, apparent surface coverage of quartz by minor Al- and Ca+Mg-bearing phases was calculated according to a monolayer model and a discrete particle model. For Al present as kaolinite ($Al_4Si_4O_{10}(OH)_8$), monolayer coverage implied a uniform coating 2.5 nm thick, but this accounted for less than 1% of the total Al in the sand measured by bulk dissolution.[3] The discrete-particle model assumed a particle thickness of 500 nm (consistent with SEM observations), and implied that approximately half of the surface area was covered by kaolinite flakes. Although surface coverage evident in SEM photomicrographs appeared to be much lower (5 – 10%), mass balance for Al was within an order of magnitude — reasonable agreement given the semi-quantitative nature of this model.

For Ca+Mg, the discrete particle model required 4% surface coverage. Because Ca+Mg constitutes only ~0.008% of the bulk sand, however, mass-balance requires that Ca+Mg must be concentrated at the grain surfaces, either as a coating or as tiny particles, and cannot be present as individual sand-sized grains of carbonate. Energy-dispersive spectrometric data acquired during SEM observations provide additional support for the coating hypothesis, as no grains rich in Ca+Mg were detected.

B. Nickel Solubility

The effective Ni solubility in batch adsorption systems must be known so that decreases in dissolved Ni due to precipitation are not attributed mistakenly to adsorption. Initially CO_2-free batch systems without adsorbent were equilibrated for 14 days in air. Dissolved Ni decreased significantly in all systems, indicating approach to equilibrium from supersaturation. A precipitate was visible in those systems with initial Ni > 10^{-2} M (initial pH < 8.5); more alkaline systems lacked sufficient Ni to produce observable precipitate. The mineralogy of the precipitate, determined by X-ray diffraction, was poorly crystalline theophrastite ($Ni(OH)_2$).

Figure 1 compares the dissolved Ni concentrations in nominally CO_2-free batch-adsorption experiments with the experimental $Ni(OH)_2$ solubility curve (this work) and curves calculated using HYDRAQL[13] with thermodynamic data given by Baeyens and McKinley.[9] Most batch-adsorption systems were quite undersaturated with respect

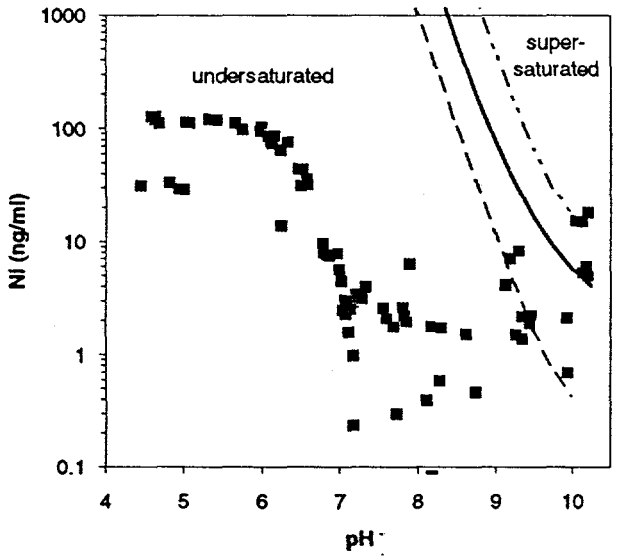

Figure 1. Comparison of final Ni concentrations in batch adsorption experiments (■) with measured Ni solubility (—) and calculated stability limits for crystalline (- -) and amorphous (– - -) $Ni(OH)_2$.

to Ni hydroxide. In these systems, decreases in dissolved Ni must have been due to adsorption. At pH values > 9, however, adsorption experiments were oversaturated with respect to crystalline $Ni(OH)_2$ but not with respect to amorphous $Ni(OH)_2$, and because of unquantified diffusion of CO_2 into the reaction tubes in these experiments, there is no clear means of discriminating between adsorption, precipitation, and carbonate-complexation effects.

C. Batch Adsorption Studies

Nickel adsorption vs. pH was measured for a variety of systems, summarized in Table 1. For untreated Wedron 510 sand, experiments investigated the effects of variations in P_{CO_2} and total Ni, the effects of competition with Li, and the effects of variations in ionic strength. A scale showing the effective K_d has been plotted for figures displaying only sand data (Figures 2 – 5). Wedron sand contains ~33 ng/g exchangeable Ni, which has been included in total soluble Ni for adsorption calculations. Experiments with synthesized goethite and with acid-washed Min-U-Sil 5 α-quartz provided adsorption curves for pure analogs of surfaces exposed by the sand.

Figure 2 displays two sets of adsorption data collected under nominally CO_2-free conditions and 100 ng/m*l* added Ni. Both sets were initially CO_2-free, but one was equilibrated on the benchtop, so ambient CO_2 may have diffused into the containers through the seals. The other was equilibrated in a nitrogen-filled glovebox. Both data sets define the same adsorption edge, located at pH 6 – 7. At pH 10 the glovebox systems showed greater adsorption (~95%) than the benchtop systems (~88%).

Variations in added Ni and P_{CO_2} are compared in Figure 3. Two data sets, partially equilibrated with air (P_{CO_2} = $10^{-3.5}$ atm), contained added Ni of 100 ng/m*l* or 200 ng/m*l*. They define an adsorption edge which is offset slightly toward lower pH in comparison with nominally CO_2-free data. Both sets appear to lie on the same curve, suggesting that the available adsorption sites were not saturated at the higher Ni concentration. At higher pH (> 9) the data show lower adsorption than the glovebox data, consistent with the trend noted in Figure 2 of decreasing adsorption with increasing P_{CO_2}. At intermediate pH values (7 – 9), adsorption is slightly higher under air-equilibrated conditions.

The competitive effect of Li on Ni adsorption is illustrated in Figure 4. These samples were run with 100 ng/m*l* added Ni and 10 μg/m*l* (0.0014 M) added Li under nominally CO_2-free conditions, or with 200 ng/m*l* added Ni, 17.4 μg/m*l* (0.0025 M) added Li, and equilibrated with air. Li was added as LiBr. In both cases, the adsorption edge was slightly broader than for Li-free conditions and was displaced slightly toward higher pH. The second set (high Li, air-equilibrated) is indistinguishable from the first, apparently due to offsetting effects of Li

Table 1. Experimental conditions for batch adsorption studies.

Electrolyte (NaCl conc.)	P_{CO_2} and ambient* atm.	Ni added (ng/m*l*)	Li added (μg/m*l*)
Wedron 510 Sand (untreated)			
0.001 M	CO_2-free, air	100	
0.001 M	CO_2-free, N_2	100	
0.001 M	air, air	100	
0.001 M	air, air	200	
0.001 M	CO_2-free, air	100	10
0.001 M	air, air	200	17
0.1 M	CO_2-free, N_2	100	
Geothite (synthetic)			
0.001 M	air, air	100	
Min-U-Sil 5 (acid-washed)			
0.001 M	CO_2-free, N_2	100	

*atmosphere surrounding tubes during equilibration.

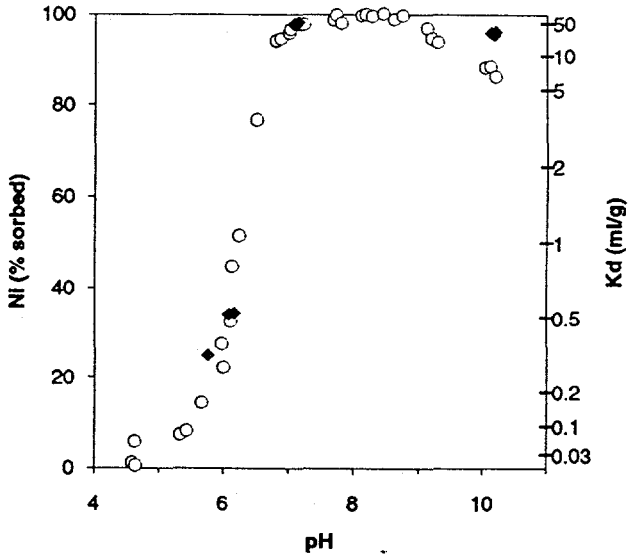

Figure 2. Adsorption of Ni by Wedron 510 sand under nominally CO_2-free conditions, 100 ng/m*l* added Ni, in 0.001 M NaCl. O = equilibrated on benchtop. ◆ = equilibrated in N_2 glovebox.

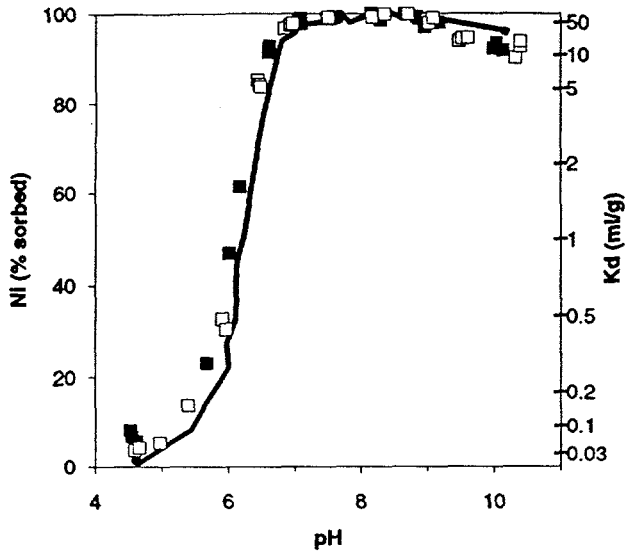

Figure 3. Variation with P_{CO_2} and added Ni: Adsorption of Ni by Wedron 510 sand under atmospheric conditions. ■ = 100 ng/m*l* Ni and □ = 200 ng/m*l* Ni. — = nominally CO_2-free data from Figure 2 (all points below pH 8.5 and glovebox-equilibrated points at pH 10).

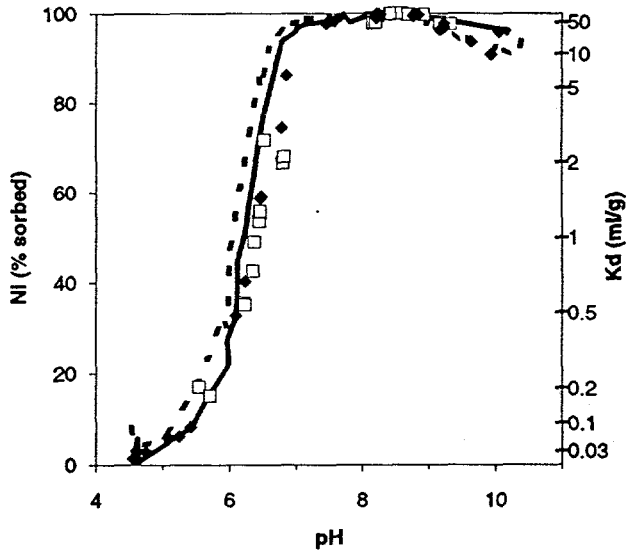

Figure 4. Competitive effect of Li: Adsorption of Ni by Wedron 510 sand in the presence of Li. ◆ = 100 ng/m*l* Ni, 10 μg/m*l* Li, CO_2-free; □ = 200 ng/m*l* Ni, 17 μg/m*l* Li, equilibrated with air. Data collected under nominally CO_2-free conditions (—), and equilibrated with air (- -) from Figures 2 and 3 shown for reference.

competition and CO_2-enhanced adsorption.

The effect of ionic strength on Ni adsorption is shown in Figure 5. Ni adsorption in 0.1 M NaCl appeared to be essentially identical to adsorption in 0.001 M NaCl for nominally CO_2-free systems.

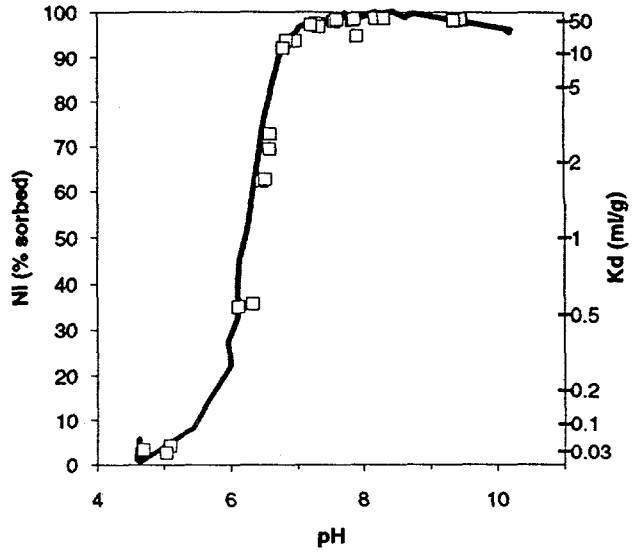

Figure 5. Variation in ionic strength: Adsorption of Ni by Wedron 510 sand in 0.1 M NaCl, nominally CO_2-free, glovebox equilibrated. □ = 100 ng/m*l* Ni. Adsorption curve for 0.001 M NaCl under nominally CO_2-free conditions (—) from Figure 3 is shown for reference.

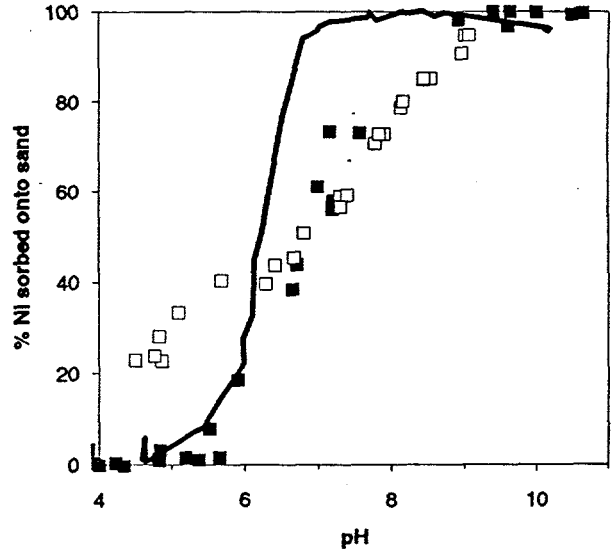

Figure 6. Comparison with pure minerals: Adsorption of Ni onto Min-U-Sil quartz (□) and synthesized goethite (■). Experimental conditions are described in Table 1. Wedron 510 CO_2-free adsorption curve (—) is shown for reference.

Adsorption of Ni onto pure quartz and goethite surfaces is shown in Figure 6. Min-U-Sil 5 α-quartz was acid-washed prior to use. Batch systems containing 0.4467 g Min-U-Sil were run under CO_2-free protocol and were equilibrated under N_2. Although the surface area of the Min-U-Sil systems was similar to that of the Wedron

systems (163 vs. 118 m^2/l), the data differ markedly. The adsorption of Ni by Min-U-Sil exhibits a very broad edge, increasing linearly with pH over the range 4.5 – 9. There was 20% adsorption at pH 5, a pH at which Wedron sand showed no significant adsorption.

In the batch sorption experiments using synthesized goethite, the amount of goethite (2.353 g) added to 20 m*l* 0.001 M NaCl contained the same quantity of Fe that could be leached with 6 N HCl from 20 g sand. The resulting systems contained a surface area of 5.59 m^2/l and a site concentration of 2.15×10^{-5} M. These systems were partially equilibrated with atmospheric CO_2 during preparation. At pH values less than ~7.5, equilibrium was probably closely approached, resulting in a partial pressure of CO_2 of nearly $10^{-3.5}$ atm, whereas at higher pH values the systems probably remained highly undersaturated due to the high solubility of CO_2. Although the upper portion of the adsorption edge is poorly constrained, the Ni-adsorption curve appears to be similar in shape but less steep than the curve for Wedron sand.

D. Potentiometric Titrations

Potentiometric titrations on quartz provides two input values for a triple-layer model of surface complexation[14] — the intrinsic equilibrium constant for proton loss by the surface (K_{a2}), and the intrinsic stability constant for complexation of the background-electrolyte cation (K_{Na}):

$$K_{a2} \equiv \text{SOH} \rightleftarrows \text{-SO}^- + \text{H}^+ \text{, and} \qquad \{1\}$$

$$K_{Na} \equiv \text{SOH} + \text{Na}^+ \rightleftarrows \text{-SONa} + \text{H}^+ \text{;} \qquad \{2\}$$

where S represents a surface site. Potentiometric titrations were performed on acid-washed Wedron 510 sand and acid-washed Min-U-Sil 5 α-quartz. Raw Wedron sand could not be potentiometrically titrated because of its carbonate content, which strongly affects the system pH as it dissolves and thus obscures the contribution of surface interactions.[3]

1. Data Reduction. Data reduction followed the double-extrapolation method.[15,16] The surface charge, σ, was calculated from charge balance considerations for the electrolyte. Double-extrapolations were performed graphically on a semi-log plot of the apparent equilibrium constant (Q) versus a linear combination of α_- (the fraction of deprotonated sites), and the ionic strength (I). Here

$$\alpha_- = \frac{-\sigma}{N_s} \cdot b \qquad \{3\}$$

where N_s is the site density in sites/nm^2 and b is a conversion factor = 0.06239 relating sites/nm^2 to $\mu C/cm^2$. For K_{a2} and K_{Na}, the respective expressions for Q_{a2} and Q_{Na} are

$$pQ_{a2} = \text{pH} - \log\frac{\alpha_-}{1-\alpha_-} \text{ , and} \qquad \{4\}$$

$$pQ_{Na} = \text{pH} - \log\frac{\alpha_-}{1-\alpha_-} + \log[\text{Na}^+] \text{ .} \qquad \{5\}$$

To find pK_{a2}, pQ_{a2} was plotted vs. $\alpha_- + c\sqrt{I}$, where c is an adjustable parameter. Each titration curve was first extrapolated to $\alpha_- = 0$, and then the resulting array of points was extrapolated to the pQ_{a2} axis, where $\alpha_- = I = 0$ and $pK_{a2} = pQ_{a2}$. The data were also extrapolated to $I = 0$ and then to $\alpha_- = 0$. A similar procedure was followed to find pK_{Na}, except that pQ_{a2} was first substituted for pQ_{Na} (allowable because $pQ_{Na} = pQ_{a2}$ at $\log I = 0$) to provide increased dispersion, and then pQ_{a2} was plotted vs. $\alpha_- + c \log I$. Finally, contour lines were double-extrapolated to $\alpha_- = 0$ and $\log I = 0$, where $pK_{Na} = pQ_{a2} = pQ_{Na}$. Precision of extrapolations for pK_{a2} is better than ± 0.2 units, controlled mainly by the data at low I. Precision for pK_{Na} is only ± 0.4 for data with maximum $I = 0.1$ M.

2. Results for Acid-Washed Min-U-Sil and Wedron 510 Sand. Double-extrapolation plots for K_{a2} and K_{Na} for acid-washed Min-U-Sil 5 are shown in Figure 7. Surface-charge calculations assumed a specific surface area of 5.95 m^2/g (multi-point Kr BET[17]), and a site density of 6 nm^{-2}. Points below pH ~4.75 were excluded because of probable systematic errors implied by the erratic trends of surface charge vs. pH. The extrapolated values are $pK_{a2} = 7.8$ and $pK_{Na} = 5.6$. The pK_{a2} value is typical of quartz, but pK_{Na} is slightly lower than normal.

Double-extrapolation results for acid-washed Wedron 510 sand are plotted in Figure 8. Surface-charge was calculated assuming a surface area of 0.12 m^2/g, (N_2-BET)[3] and a site density of 6 nm^{-2}, matching that of the Min-U-Sil. The extrapolated values are $pK_{a2} = 5.5$ and $pK_{Na} = 4.8$, much lower than typically seen for quartz.

IV. DISCUSSION

A. Surface Characteristics Implied by Potentiometric Titrations

A comparison of batch titration curves for raw Wedron 510 sand, acid-washed Wedron 510 sand, and acid-washed Min-U-Sil 5 α-quartz suggested that the potentiometric titration curves of the raw sand were dominated

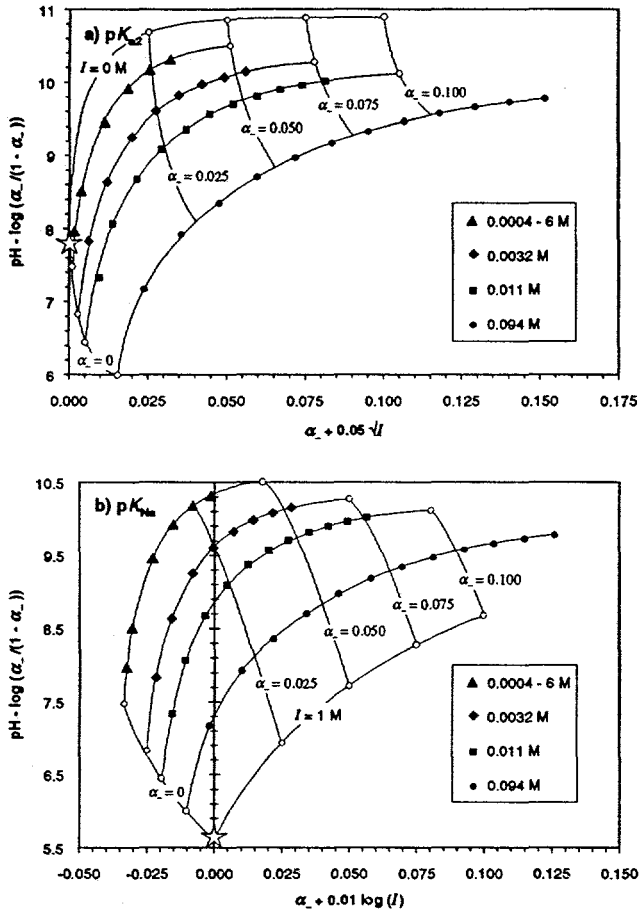

Figure 7. Double-extrapolation plots for HCl-washed Min-U-Sil 5. a) Extrapolation for pK_{a2}, giving a value of 7.8. b) Extrapolation for pK_{Na}, giving a value of 5.6.

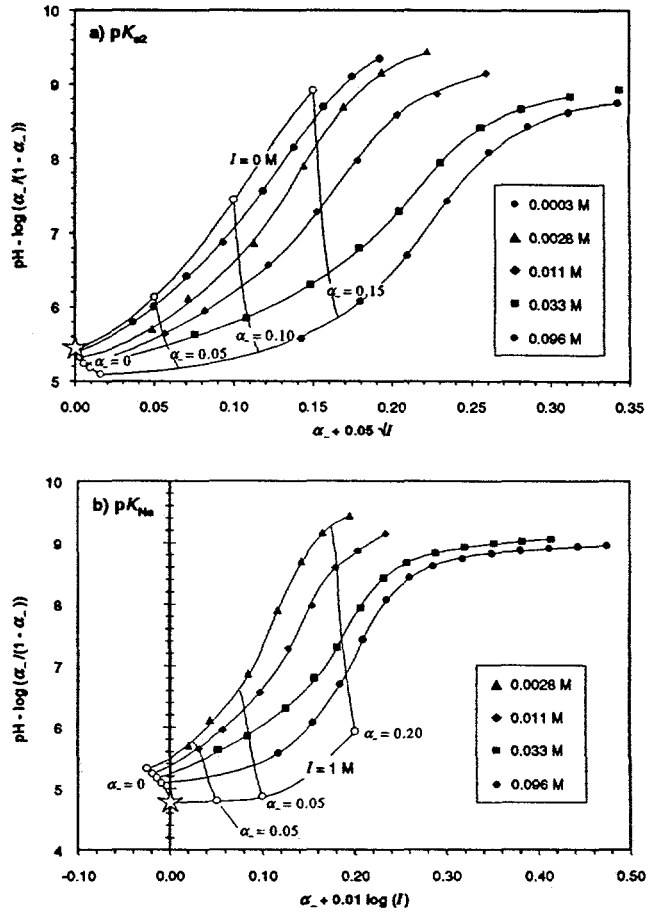

Figure 8. Double-extrapolation plots for acid-washed Wedron 510 sand. (a) Extrapolation for pK_{a2}, giving a value of 5.5. (b) Extrapolation for pK_{Na}, giving a value of 4.8.

by the effects of carbonate dissolution and CO_2 uptake.[3] Washing in boiling HCl stripped the sand grains of their coatings, resulting in a batch titration curve that qualitatively resembled that for acid-washed Min-U-Sil 5 quartz.[3]

Potentiometric titrations and related surface-charge calculations for acid-washed Min-U-Sil provide a standard for surface properties expected for quartz. Double-extrapolation plots and derived values (pK_{a2} and pK_{Na}) for Min-U-Sil are within the range of values reported in the literature for this material[17,18,19] and other forms of silica.[16] In contrast, surface-charge calculations and double-extrapolation plots for Wedron sand give much different results. Calculated charge density was unusually high for all ionic strengths, with the apparent charge density at pH 9 of 50 $\mu C/cm^2$ implying deprotonation of more than 30% of the available surface sites. With increasing pH, the increase in charge density was quite small, and with increasing I, the displacement toward higher charge was unusually small as well.

The intrinsic association constants, K_{a2} and K_{Na}, were much greater than those for Min-U-Sil; pK_{a2} = 5.5 vs. 7.8 and pK_{Na} = 4.8 vs. 5.6 respectively. Combined with the high surface charge noted above, this suggests that the surface area may have been much larger than the N_2-BET value. A source of additional surface area may have been the colloidal suspension of kaolinite that appeared as the pH was increased. The specific surface area of the kaolinite is not known, but Xie and Walther[20] propose an effective surface area of 101 m^2/g and a site density of 19.8 nm^{-2} for a kaolinite from Washington County, Georgia in order to account for its titration behavior. If a site density of 6 nm^{-2} is assumed for consistency with the double-extrapolation calculations, the equivalent surface area for this kaolinite would be 333 m^2/g. Because kao-

linite constitutes ~0.05% by weight of the sand,[3] it could contribute 0.17 m^2 per gram of bulk sand, more than doubling the surface area in solution. Even so, a high degree of deprotonation and unusually strong Na binding are still implied.

The potentiometric titrations have shown that development of surface charge on the sand is only poorly understood. In spite of acid-washing for quantitative removal of carbonate and Fe-oxyhydroxide phases, the average surface of Wedron sand did not resemble quartz but instead must have included a variety of sites, with poorly constrained site density and effective surface area. Such complexity will be difficult to unravel by potentiometric titration.

B. Ni Adsorption

1. Summary of Experimental Observations. Under both atmospheric P_{CO_2} and CO_2-free conditions, Ni was not adsorbed appreciably by the Wedron 510 sand below a pH of 5 in NaCl electrolyte. Adsorption increased with pH, with a steep adsorption edge between 6.0 and 7.0; by pH 7.0, adsorption was >99%. Nearly all Ni was adsorbed from pH 7.0 to 9.0, but as pH increased above 9.0, adsorption slowly decreased. Doubling the amount of Ni added from 100 ng/m*l* (1.7×10^{-6} M) to 200 ng (3.4×10^{-6} M) had no measurable effect on adsorption; neither did increasing the ionic strength by a factor of 100 from 0.001 M to 0.1 M. These observations suggest that only a small fraction of the available sites are occupied by Ni, and that competition with Na for sites is not a significant factor determining Ni adsorption.

Addition of large amounts of Li as LiBr (0.0014 – 0.0025 M) interfered with Ni sorption, shifting the sorption edge toward higher pH by ~0.2 pH units for 0.0014 M Li. Lithium has been shown to adsorb only weakly onto the sand at this concentration,[3] exhibiting a K_d of ~0.2 (17% sorption) for batch systems with a 1:1 solution:solid ratio. Although addition of Li increased the ionic strength by a factor of two to three, Ni adsorption is insensitive to such variations (see above). Possible mechanisms that explain the decreased adsorption of Ni are: (1) Competition between Li and Ni for adsorption sites, or (2) Stabilization of Ni is solution by complexation with Br^-. Given the geochemical similarity between Br^- and Cl^-, the former appears most likely.

Similar Ni adsorption curves have been reported in the literature. Richter[21] measured Ni adsorption onto 50 m^2/l goethite or quartz at ionic strengths ranging from 0.001 to 0.1 M $NaClO_4$ with 1 μg/m*l* total Ni. Adsorption on quartz showed a pattern similar to that seen for Min-U-Sil 5 quartz in the present study, but included a pronounced decrease in adsorption with increasing ionic strength. Adsorption on goethite was remarkably similar to that seen here for Wedron 510 sand, with adsorption beginning at pH 6 and nearly complete by pH 7, and with no discernible effect due to variations in ionic strength. Dzombak and Morel[22] report adsorption curves for Ni onto hydrous ferric oxide (total Fe = 10^{-3} M) in 0.1 M $NaNO_3$ at total Ni = 5×10^{-7} and 5×10^{-6} M. The surface area was probably near 60 m^2/l, so conditions resembled those for Wedron sand. However, their adsorption curves did not resemble those for the sand as closely as did Richter's. Adsorption exceeded 10% by pH 6 but increased less steeply with pH than did adsorption onto the sand. Increasing Ni by an order of magnitude shifted the adsorption edge to slightly higher pH by ~0.2 units.

Increasing the P_{CO_2} produced a shift in the adsorption curve (Figures 2 and 3). At pH 5 – 8, adsorption of Ni was enhanced, shifting the adsorption edge to lower pH by ~0.2 pH units; whereas at higher pH, the degree of adsorption decreased with increasing P_{CO_2} in the system. Actual P_{CO_2} can only be qualitatively inferred; for all systems at low pH, carbonate dissolution in the sand led to increased P_{CO_2}, whereas in air-equilibrated systems above pH 8, lack of equilibration with atmospheric CO_2 resulted in a P_{CO_2} less than $10^{-3.5}$ atm by an unknown amount. In nominally CO_2-free systems, a small amount of CO_2 appears to have diffused through the cap seals for those systems equilibrated on the benchtop, surrounded by air. The enhanced adsorption seen at pH < 8 may be due to binding of a Ni-carbonato complex or to adsorption of CO_2 to create a surface site that resembles a carbonate ligand which then readily binds Ni. Decreased adsorption at high pH with increased P_{CO_2} may be due to formation of stable Ni-carbonato complexes in solution, or may be related to the dispersed colloids present at high pH. Some colloidal particles may pass through the 0.2 μm filter; any adsorbed Ni on such particles would then contribute to the total Ni measured by GFAA.

2. Modeling. The adsorption of Ni^{2+} onto Wedron sand closely resembles that of synthesized goethite, suggesting that goethite alone may serve as an analog for the more complex sand for modeling purposes. Goethite, synthesized by the same methods used here, has been extensively studied for its surface properties, so input parameters for surface-complexation modeling were ob-

Table 2. Parameters held constant for modeling Ni adsorption onto synthesized goethite and Wedron sand using the triple-layer model. K_{int} = intrinsic equilibrium constant, S = surface site.

1. Properties of Goethite	Value	Ref.
Specific surface area	48.5 m²/g	24
Site density	2.31 sites/nm²	25
Inner-layer capacitance	0.8 F/m²	13
Outer-layer capacitance	0.2 F/m²	26
2. Speciation of Ni^{2+}	**log K**	**Ref.***
$Ni^{2+} + Cl^- == NiCl^+$	0.4	27
$Ni^{2+} + 2Cl^- == NiCl_2$	0.96	27
$Ni^{2+} + OH^- == NiOH^+$	-9.9	28
$Ni^{2+} + 2OH^- == Ni(OH)_2$	-18.2	29
$Ni^{2+} + 3OH^- == Ni(OH)_3^-$	-30	30
$Ni^{2+} + 4OH^- == Ni(OH)_4^{2-}$	-44	30
$2Ni^{2+} + 3OH^- == Ni_2(OH)_3^+$	-10.7	30
$4Ni^{2+} + 4OH^- == Ni_4(OH)_4^{4+}$	-27.74	30
$Ni^{2+} + CO_3^{2-} == NiCO_3$	6.87	27
$Ni^{2+} + 2CO_3^{2-} == Ni(CO_3)_2^{2-}$	10.11	27
$Ni^{2+} + HCO_3^- == NiHCO_3^+$	12.47	27
3. Surface complexes	**log K_{int}**	**Ref.**
$SOH == SO^- + H^+$	-9.52	24
$SOH + H^+ == SOH_2^+$	5.57	24
$SO^- + Na^+ == SO\text{-}Na$	-8.4	24
$SOH_2^+ + Cl^- == SOH_2\text{-}Cl$	7	24

* values recommended by Baeyens and McKinley[9]. Original sources are cited here.

tained from the published literature (listed in Table 2, part 1).

Modeling was performed using the triple-layer model[14,23] (TLM) as implemented in the HYDRAQL[13] code. HYDRAQL includes an extensive thermodynamic database that lists formation constants for most common complexes. This database was augmented by more detailed Ni speciation data from a variety of sources, as presented in the part 2 of Table 2. These data were critically evaluated by Baeyens and McKinley[9] for internal consistency and sound experimental design.

Surface complexation constants for goethite, listed as intrinsic equilibrium constants in part 3 of Table 2, were obtained by Balistrieri and Murray[24] from potentiometric titration data using the double-extrapolation method. They used a site density of 2.56 sites/nm^2 in their calculations, but because the double-extrapolation method extrapolates to zero surface charge ($\alpha_- = 0$), it is insensitive to variations in the assumed site density. The protonation and deprotonation reactions imply a pH of zero net proton charge (pH_{ZNPC}) of 7.54 for the goethite surface.

The experimental adsorption data for goethite were modeled by assuming one or more surface-complexation reactions between dissolved species and a surface site, and then adjusting the intrinsic equilibrium constants to obtain a good visual fit. This set of parameters was then used to model the experimental observations on the sand by adjusting the surface area (and hence the site concentration in solution) to again obtain a good visual fit. Finally, the effects of ionic strength were examined by comparing model predictions to experimental data on sand in 0.1 M NaCl.

HYDRAQL was used to calculate Ni speciation in the absence of adsorbent under both atmospheric CO_2 conditions ($P_{CO_2} = 10^{-3.5}$ atm) and very low CO_2, where $P_{CO_2} = 10^{-6}$ atm. Results are shown in Figure 9. Under atmospheric conditions (Figure 9a), Ni-carbonato complexes predominate at pH values above 7.5, where Ni is strongly sorbed. Under low-CO_2 conditions, however, the predominance of Ni-carbonato complexes occurs only above pH 8.5, whereas the abundance of Ni-hydroxyl complexes is much greater. These differences in speciation are critical to developing a realistic model of the experimental data.

A range of possible surface complexes was modeled, as summarized in Table 3. Both monodentate (complexation to a single site) and bidentate (complexation to two sites) adsorption were considered. Possible sorbing species included Ni^{2+} or $NiOH^+$ as either inner-sphere or outer-sphere complexes, and various Ni-carbonato species as outer-sphere complexes. Inner-sphere complexes are closely bound, with the surface site replacing one of the water molecules in the innermost hydration shell. Outer-sphere complexes are more distantly bound, leaving the innermost hydration shell intact.

Models of adsorption of the Ni-carbonato species were unable to reproduce the experimental data. Curves for two possible adsorbed Ni-carbonato complexes are

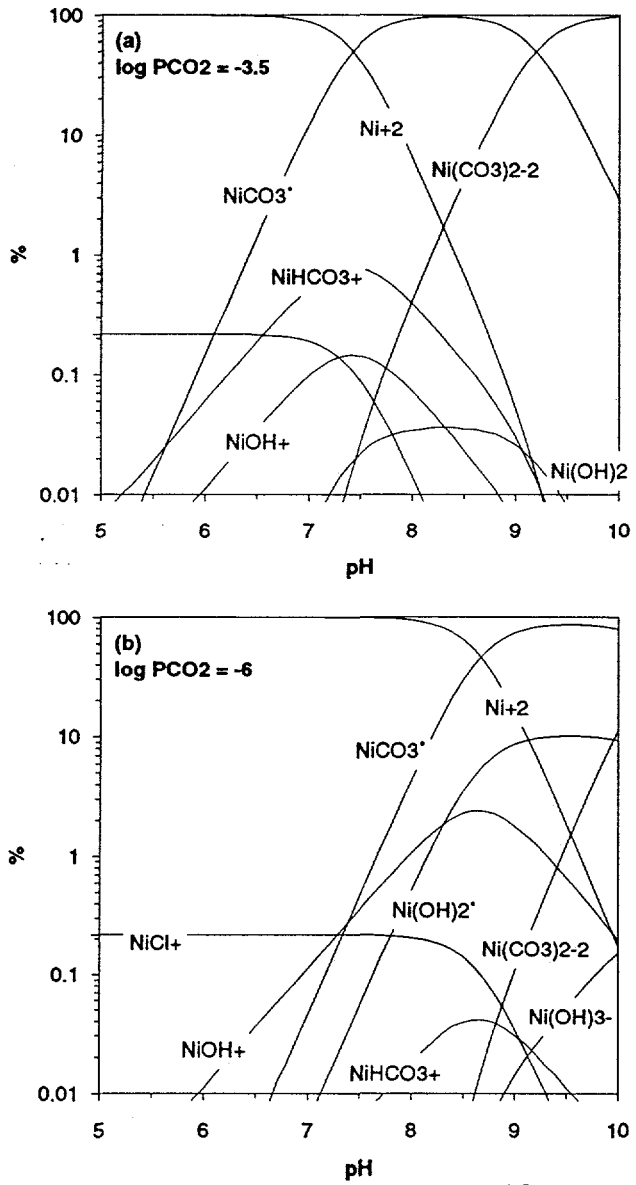

Figure 9. Nickel speciation. a) $P_{CO_2} = 10^{-3.5}$ atm. b) $P_{CO_2} = 10^{-6}$ atm.

shown in Figure 10 for atmospheric CO_2 ($P_{CO_2} = 10^{-3.5}$ atm). Formation of the $SONiCO_3^-$ complex depends only on the concentration of the reactants, SO^- and $NiCO_3^0$, but is unaffected by surface charge; the sorption edge is located where the reactants become important species. Formation of the $SONi(CO_3)_2^{3-}$ requires that the chemical interaction be strong enough to overcome a countervailing electrostatic contribution above the pH_{ZNPC}, which results in a very broad sorption edge at low pH. For the curves shown, binding constants were adjusted to reproduce the adsorption edge. Increasing the binding constant (K_{int}) increases the maximum adsorption but shifts the adsorption edge to lower pH, resulting in poorer fits.

Table 3. Investigated surface complexes.

	Surface Sites	
Sorbing Species	SO^-	$(SO^-)_2$
Inner Sphere		
Ni^{2+}	X	X
$NiOH^+$	X	
Outer Sphere		
Ni^{2+}	X	X
$NiOH^+$	X	
$NiCO_3^0$	X	
$Ni(CO_3)_2^{2-}$	X	
$NiHCO_3^+$	X	
$NiH_2CO_3^{2+}$	X	

The most successful model involved the formation of an inner-sphere complex between Ni^{2+} and a single SO^- site, with an intrinsic equilibrium constant of 10^{-1}. This is also the stoichiometry recommended by Dzombak and Morel.[22] Results are shown in Figure 11 for $P_{CO_2} = 10^{-3.5}$ and 10^{-6} atm. At low pH, the calculated adsorption curves are insensitive to variations in P_{CO_2}, but at pH > 7 the calculated curves begin to diverge. At $P_{CO_2} = 10^{-3.5}$ atm, adsorption reaches a maximum of only 83% at pH 8.2 and then shows decreasing sorption at higher pH due to formation of stable Ni-carbonato complexes in solution. Maximum calculated adsorption could be increased by postulating a larger intrinsic equilibrium constant, but this would also shift the calculated adsorption edge to lower pH. A more satisfactory alternative is to assume that the batch systems at high pH were greatly undersaturated with respect to CO_2. A CO_2 partial pressure of 10^{-6} atm is the maximum CO_2 level compatible with the experimental data.

Application of this model using low P_{CO_2} to experimental data for Wedron sand is shown in Figure 12. Good agreement is obtained by setting the goethite surface area to 65 m^2/l. Increasing the ionic strength in the calculations by two orders of magnitude to 0.1 M shifts the calculated sorption edge to higher pH by only 0.2 pH units. This small shift is due to coordination of Ni^{2+} as an inner-sphere complex; the calculated sorption edge is consistent with experimental observations. In contrast,

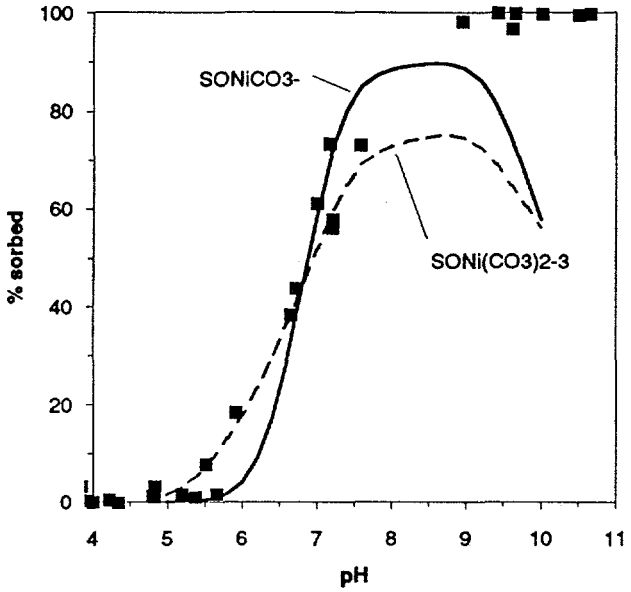

Figure 10. Calculated adsorption of Ni-carbonato complexes onto synthesized goethite at $P_{CO_2} = 10^{-3.5}$ atm. Experimental conditions: surface area = 5.59 m²/liter; electrolyte = 0.001 M NaCl; total Ni = 100 ng/ml (1.7×10^{-6} M); partially equilibrated with atmospheric CO_2.

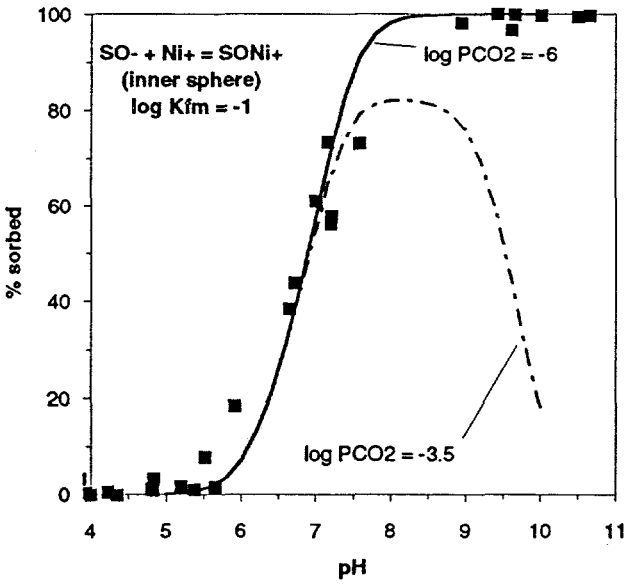

Figure 11. Calculated adsorption of Ni^{2+} onto synthesized goethite for two partial pressures of CO_2. Experimental data are the same as in Figure 10.

outer-sphere complexes are quite sensitive to variations in ionic strength; all outer-sphere models of Ni complexation showed much greater shifts toward lower pH, leading to their rejection. The behavior of Ni in the presence of Li lends further support to the inner-sphere hypothesis. Although Li was present at molar concentrations greater

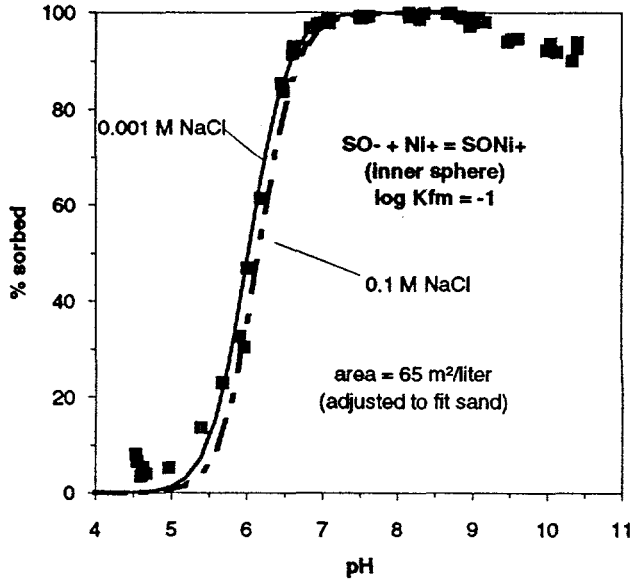

Figure 12. HYDRAQL modeling of Ni sorption onto Wedron sand using TLM parameters for goethite. Model curves: — = 0.001 M NaCl, — - = 0.1 M NaCl. Experimental data (■): surface area = 120 m^2/l; electrolyte = 0.001 M NaCl; total Ni = 133 ng/ml (2.3×10^{-6} M); partially equilibrated with atmospheric CO_2.

than Ni by a factor of 1000, it competed only weakly with Ni for adsorption sites. Lithium probably forms an outer-sphere complex with the sand, consistent with its comparatively weak adsorption. If Ni had formed an outer-sphere complex, it would have been displaced more readily by Li.

The specific surface area of the Fe-bearing phase postulated for the sand is quite high — the amount of Fe which as synthetic goethite gave a surface area of 5.59 m^2/l must be spread thinly enough to provide a surface area of 65 m^2/l. Thus its specific surface area would be: 48.5 m^2/g * (65 m^2/l / 5.59 m^2/l) = ~560 m^2/l. Such a value is probably inconsistent with occurrence as goethite, but both ferrihydrite and amorphous $Fe(OH)_3$ can have such high specific surface areas, and have surface complexation constants similar to those of goethite.[22]

The total surface area of the Wedron sand in the batch systems is estimated to have been ~120 m^2/l, based on N_2-BET data for the sand and a 1:1 solid:solution ratio. Thus the postulated Fe oxyhydroxide phase with a surface area of 65 m^2/l would account for 54% of the available surface area. It is possible that Fe-oxyhydroxides coat most of the surfaces in the sand and hence dominate the adsorptive properties. Alternatively, the actual surface

area of the sand available for sorption may be much greater, as suggested by the potentiometric titrations as described in section IV(A). Another possibility is that the bulk adsorptive behavior of the sand is due to adsorption onto at least three types of surfaces: Fe-oxyhydroxide, kaolinite, and quartz.

3. Implications for Transport Calculations. In heterogeneous groundwater systems, adsorption may be controlled by trace amounts of reactive minerals or coatings of inert materials that are preferentially concentrated along flow paths or other structural features. Both proper characterization of mineral surfaces and formulation of an adsorption model for mixtures of minerals are required for site characterization because studies of metal adsorption by bulk rocks may not provide information about the most important adsorption sites. It is important for performance assessment calculations to determine if radionuclide discharges could be substantially different from those calculated using K_d values obtained from the bulk rock.

The caisson experiment provides an opportunity to evaluate alternative approaches to predict the sorption properties of natural mineral mixtures. Approaches applied in previous studies of synthetic materials have ranged from simple linear additivity models to multi-site surface complexation models.[31] The modeling exercise described above shows that the TLM can successfully simulate the adsorptive behavior of Wedron sand with respect to Ni in a simple batch system without competing adsorbates. The data describing Ni adsorption onto goethite were examined to obtain the stoichiometries of possible adsorption reactions and associated binding constants. The most important system parameter is pH, followed by surface area (and hence site concentration). These results were then applied to the data for Ni sorption onto Wedron sand, where the model fit to the observations was optimized by adjusting the postulated surface area of goethite. Although the model is not rigorously based on the behaviors of the constituent components of the sand, it does simulate the aggregate behavior of the bulk sand and will be useful for transport calculations.

Several points are in need of further refinement, however: 1) Experimental evidence shows that at low to neutral pH Ni adsorption by the sand is slightly enhanced by the presence of CO_2, implying the existence of a Ni-carbonato surface complex. As noted above, however, inclusion of such complexes resulted in poor model behavior at $P_{CO_2} = 10^{-3.5}$ atm. This failure may be due to inadequate knowledge of the partial pressure of CO_2 in the goethite experiments where P_{CO_2} was lower by an unknown amount, or possibly due to inadequacies of the thermodynamic data for Ni-carbonato complex formation. 2) The ability of the model to predict the weakly competitive effect of Li needs to be examined. 3) The electrolyte being used in the caisson is not pure 0.001 M NaCl, but rather is tapwater with significant concentrations of divalent cations. Such cations (Ca^{2+} and Mg^{2+}, principally) may exhibit chemical as well as electrostatic interactions with the sand surface, thus competing with Ni^{2+} for adsorption sites.

V. SUMMARY

The surface chemistry of a quartz sand (Wedron 510 sand) that will be used in an intermediate scale transport experiment has been studied. XRD and leaching studies indicate that the surface of the sand is partially covered by Fe-oxyhydroxide, kaolinite, and Ca-Mg carbonate. Previous studies by SEM failed to reveal any grains or particles rich in Fe or Ca+Mg, even in the colloidal fraction, implying that the sources of these elements (Fe-oxyhydroxide and carbonate) occur as thin coatings or as fine particles adhering to the grains of sand. Modeled distributions of Ca and Mg based on XPS data favor an extremely dispersed mode of occurrence as well. In order to account for the observed surface concentration of Ca and Mg while observing mass balance constraints (acid-leachable Ca+Mg is only 1.03 μmole/g), Ca and Mg must be concentrated at the immediate surface of the sand grains, either as a coating or as particles much less than 500 nm in large dimension (otherwise they would have been detected by SEM/EDS). The Al in kaolinite was also detected by XPS. The intense signal implied that as much as half the available surface might be covered by kaolinite flakes. Such a distribution is consistent with SEM observations on the morphology of the colloidal fraction and accounts for the Al content of the sand.

Potentiometric titrations on the sand differ from those of pure quartz and suggest that the effective surface area of the sand measured by N_2-BET gas adsorption (0.118 m^2/g) may seriously underestimate the actual area exposed to solutions. The untreated sand is probably too complex to investigate using potentiometric titrations.

A surface-complexation model of Ni adsorption by the sand has been formulated for use in transport calculations using the LEHGC code. Batch adsorption studies show that Ni adsorption is strongly pH-dependent, changing from 20% adsorbed at pH 6 to complete adsorp-

tion at pH 7. Adsorption is independent of ionic strength, and is enhanced by higher levels of CO_2 below pH 8. At higher pH values, higher levels of CO_2 appear to stabilize Ni in solution. High concentrations of Li, a weakly adsorbing cation, reduce Ni adsorption slightly. Ni adsorption edges for goethite and quartz, two components of the sand were also measured. Ni adsorption on pure quartz is only moderately pH-dependent and differs in shape and location from that of the sand, whereas Ni adsorption by goethite is strongly pH-dependent.

Triple-layer surface-complexation model constants were obtained from the adsorption data for goethite using the HYDRAQL speciation code. Attempts to model the adsorption characteristics of the bulk sand in terms of the properties of pure end member components suggested that much of the sand surface is inert. The goethite model provides a good fit to the Ni-adsorption curve of the sand when the specific surface area of the Fe-oxyhydroxide coating on the sand is assumed to be ~560 m^2/g, compatible with its occurrence as amorphous Fe-oxyhydroxide. Ni adsorption mechanisms have not been unambiguously identified; however, this preliminary adsorption model provides an initial set of parameters that can be used in transport calculations.

ACKNOWLEDGMENTS

The authors are grateful to A. Sault (SNL) who performed the XPS analyses calculations under the QA direction of MDS. The assistance of C. Boyle and E. Henry (University of New Mexico), and reviews of P. Brady and V. Tidwell (both SNL) are gratefully acknowledged. The continuing support of E. Springer (LANL) is, as always, appreciated. The data included in this report are not qualified. This work was performed for the U.S. Department of Energy under Contract DE-AC04-94AL85000; under WBS 1.2.5.4.6, Q.A.G.R. 1.2.1.4.6. Rev 0 and WA-95 Rev. 00.

REFERENCES CITED

1. M.D. Siegel, "Towards A Realistic Approach To Validation Of Reactive Transport Models For Performance Assessment," *Proc. FOCUS 93, Site Characterization and Model Validation*, American Nuclear Society , Las Vegas, NV, September 26-29, 1993.

2. M.D. Siegel, P.L. Hopkins, R.J. Glass, and D.B. Ward, "Design of an Intermediate-Scale Experiment to Validate Unsaturated-Zone Transport Models," *Proc. 1992 Inter. Conf. High Level Rad. Waste Mgmt.*, p. 1972-1984, American Nuclear Society, La Grange Park, IL, 1992.

3. M.D. Siegel, D.B. Ward, W.C. Cheng, C. Bryan, C.S. Chocas, and C.G. Reynolds, "Preliminary Characterization of Materials for a Reactive Transport Model Validation Experiment," *Proc. 1993 Inter. Conf. High Level Rad. Waste Mgmt.*, held at Las Vegas, NV, April 27-30, 1993.

4. E.P. Springer, M.D. Siegel, P.L. Hopkins, and R.J. Glass, "Testing Models of Flow and Transport in Unsaturated Porous Media," *Proc. 1993 Inter. Conf. High Level Rad. Waste Mgmt.*, p. 336-347, American Nuclear Society, La Grange Park, IL, 1993.

5. S. Brunauer, P.H. Emmett, and E. Teller, "Adsorption of Gases in Multimolecular Layers," *J. Am. Chem. Soc.*, **60**, 309-319 (1938).

6. G. Zyvoloski, Z. Dash, and S. Kelkar, *FEHMN 1.0: Finite Element Heat and Mass Transfer Code*, LA-12062-MS, Los Alamos National Laboratory, Los Alamos, NM (1991).

7. G.T. Yeh and V.S. Tripathi, *HYDRO-GEOCHEM: A Coupled Model of HYDROlogic Transport and GEOCHEMical Equilibria in Reactive Multicomponent Systems*, ORNL-6371, Oak Ridge National Laboratories, Oak Ridge, TN (1990).

8. R.G. Bates, *Determination of pH*, John Wiley & Sons, Inc., New York, 479 p. (1973).

9. B. Baeyens and I.G. McKinley, *A PHREEQE Database for Pd, Ni and Se*, PSI-Bericht Nr. 34, Paul Scherrer Institut, CH, Switzerland, 59 p. (1989).

10. R.J. Atkinson, A.M. Posner, and J.P. Quirk, "Adsorption of Potential-Determining Ions at the Ferric Oxide-Aqueous Electrolyte Interface," *J. Phys. Chem.*, **71**, 550-558 (1967).

11. V.S. Tripathi, *Uranium (VI) Transport Modeling: Geochemical Data and Submodels*, unpub. Ph.D. thesis, Stanford Univ. Dept. of Applied Earth Science, Stanford, CA, 297 p. (1983).

12. M.H. Koppelman and J.G. Dillard, "A Study of the Adsorption of Ni(II) and Cu(II) by Clay Minerals," *Clays and Clay Minerals*, **25**, 457-462 (1977).

13. C. Papelis, K.F. Hayes, and J.O. Leckie, *HYDRAQL: A Program for the Computation of Chemical Equilibrium Composition of Aqueous Batch Systems Including Surface-Complexation Modeling of Ion Ad-*

sorption at the Oxide/Solution Interface, Tech. Report 306, Stanford Univ. Dept. of Civil Eng., Stanford, CA, 130 p. (1988).

14. D.E. Yates, S. Levine, and T.W. Healy, "Site-Binding Model of the Electrical Double Layer at the Oxide/Water Interface," *J. Chem. Soc. London Faraday Trans.*, **70**, 1807-1818 (1974).

15. R.O. James, J.A. Davis, and J.O. Leckie, "Computer simulation of the conductometric and potentiometric titration of the surface groups of ionizable latexes," *J. Colloid Interface Sci.*, **65**(2), 331-344 (1978).

16. D.B. Kent, V.S. Tripathi, N.B. Ball, J.O. Leckie, and M.D. Siegel, *Surface-Complexation Modeling of Radionuclide Adsorption in Subsurface Environments*, SAND86-7175, Sandia National Laboratories, Albuquerque, NM, 113 p. (1988).

17. M. Kohler and J.O. Leckie, *Neptunium(V) Sorption on Quartz and Albite in Aqueous Suspension*, Annual Progress Report for LANL Contract 9X69-1818X-1, Stanford Univ. Dept. of Civil Eng., 15 p. (1991).

18. M.G. MacNaughton and R.O. James, "Adsorption of Aqueous Mercury (II) Complexes at the Oxide/Water Interface," *J. Colloid Interfacial Sci.*, **47**, 431-440 (1974).

19. M.M. Benjamin and J.O. Leckie, "Adsorption of Metals at Oxide Interfaces: Effects of the Concentrations of Adsorbate and Competing Metals," *Contaminants and Sediments Volume 2: Analysis, Chemistry, Biology*, R.A. Baker, ed., Ann Arbor Science Publishers, Inc., Ann Arbor, MI, 627 p., 1980.

20. Z. Xie and J.V. Walther, "Incongruent Dissolution and Surface Area of Kaolinite," *Geochim. Cosmochim. Acta*, **56**, 3357-3363 (1992).

21. R.O. Richter, *Chemical Speciation of Fly Ash Pond Leachate in the Underlying Soil/Water System with Emphasis on the Adsorption of Nickel by Oxides*, unpublished Ph.D. thesis, Univ. Notre Dame, Notre Dame, IN, 208 p. (1978).

22. D.A. Dzombak and F.M.M. Morel, *Surface Complexation Modeling*, John Wiley & Sons, Inc., New York, 393 p. (1990).

23. J.A. Davis, R.O. James, and J.O. Leckie, "Surface Ionization and Complexation at the Oxide-Water Interface. 1. Computation of Electrical Double Layer Properties in Simple Electrolytes," *J. Colloid Interface Sci.*, **63**(3), 480-499 (1978).

24. L.S. Balistrieri and J.W. Murray, "The Surface Chemistry of Goethite (alpha FeOOH) in Major Ion Seawater," *Am. J. Sci.*, **281**, 788-806 (1981).

25. J.A. Davis and D.B. Kent, "Surface Complexation Modeling in Aqueous Geochemistry, in Mineral-Water Interface Geochemistry," *Reviews in Mineralogy*, v. 23, M.F. Hochella and A.F. White, eds., p. 177-260, Mineralogical Society of America, Washington, D.C., 1990.

26. R.O. James and G. Parks, "Characterization of Aqueous Colloids by their Electrical Double-Layer and Intrinsic Surface Chemical Properties," *Surface and Colloid Science*, **12**, 119-216 (1982)

27. J.W. Ball, D.K. Nordstrom, and E.A. Jenne, *Additional and Revised Thermochemical Data and Computer Code for WATEQ2 -- A Computerized Model for Trace and Major Element Speciation and Mineral Equilibria of Natural Waters*, WRI 78-116, U.S. Geological Survey Water Resources Investigations (1980).

28. D.D. Wagman, "The NBS Tables of Chemical Thermodynamic Properties: Selected Values for Inorganic and C1 and C2 Organic Substances in SI Units," *J. Phys. Chem. Ref. Data*, **11**(2), 1-392 (1982).

29. R.M. Smith and A.E. Martell, *Critical Stability Constants: Volume 4. Inorganic Complexes*, Plenum Press, New York, 257 p. (1976).

30. C.F. Baes, Jr. and R.E. Mesmer, *The Hydrolysis of Cations*, John Wiley and Sons, New York, 489 p. (1976).

31. V.S. Tripathi, M.D. Siegel, and Z.S. Kooner, "Measurement of Metal Adsorption in Oxide-Clay Mixtures: 'Competitive-Additivity' Among Mixture Components," *Scientific Basis for Nuclear Waste Management XVI*, C.G. Interrante and R.T. Pabalan, eds., Materials Research Society Symposium Proceedings v. 294, 1993.